

## Article

# Experimental Investigation on Solar Water Heater Integrated with Thermal Battery Using Phase Change Material and Porous Media

Mohammad Sajad Naghavi Sanjani <sup>1,2,\*</sup> , Mahyar Silakhori <sup>3,\*</sup> , Bee Chin Ang <sup>4</sup> ,  
Hendrik Simon Cornelis Metselaar <sup>1</sup> , Sayed Mohammad Mousavi Gazafroudi <sup>5</sup> and Younes Noorollahi <sup>2</sup> 

<sup>1</sup> Center of Advanced Materials, Department of Mechanical Engineering, Faculty of Engineering, Universiti Malaya, Kuala Lumpur 50603, Malaysia; h.metselaar@um.edu.my

<sup>2</sup> Energy Modelling and Sustainable Energy System (METSAP) Research Lab, Faculty of New Sciences and Technologies, University of Tehran, Teheran 1416634793, Iran; noorollahi@ut.ac.ir

<sup>3</sup> Center for Energy Technology, School of Electrical and Mechanical Engineering, University of Adelaide, Adelaide, SA 5005, Australia

<sup>4</sup> Department of Chemical Engineering, Faculty of Engineering, Universiti Malaya, Kuala Lumpur 50603, Malaysia; amelynang@um.edu.my

<sup>5</sup> School of Railway Engineering, Iran University of Science and Technology, Teheran 1417935840, Iran; sm\_mousavi@iust.ac.ir

\* Correspondence: sajad.naghavi@um.edu.my (M.S.N.); mahyar.silakhori@adelaide.edu.au (M.S.)

**Abstract:** Evacuated tube heat pipe solar collector as a passive solar water heating system is a simple, reliable, and cost-effective way to capture the sun's thermal energy to supply hot water to homes. In the proposed system, the manifold is reshaped to a tank and filled with phase change materials (PCM) and porous media, which the PCM acts as a latent heat thermal energy storage medium. In order to increase the heat flux from the heat pipe to the PCM and overcome the low thermal conductivity of the PCM, porous media is used. The porous media is connected to the heat pipe condenser to collect the heat and distribute it uniformly throughout the PCM filling the pores. This design of the manifold acts as a heat storage tank or thermal battery. Another pipe in the tank transfers heat from the PCM to the water. Experiments were conducted in 2 modes: charging/discharging and periodic draw-off. The results demonstrated that this thermal battery design could provide homes with the hot water they require on sunny days, while it needs an auxiliary heater or larger solar collector to provide enough hot water on rainy/cloudy days. Considering the solar radiation fluctuation, the efficiency of the thermal battery is  $50\% \pm 9.3\%$ . The thermal battery can warm up the cold water higher than the operating temperature on a sunny day (more than 120 L per day at 38 °C). Using porous media provides better heat distribution in the PCM.

**Keywords:** solar water heater; phase change material; porous media; latent heat storage; thermal battery; domestic application



check for updates

**Citation:** Naghavi Sanjani, M.S.; Silakhori, M.; Ang, B.C.; Simon Cornelis Metselaar, H.; Mousavi Gazafroudi, S.M.; Noorollahi, Y. Experimental Investigation on Solar Water Heater Integrated with Thermal Battery Using Phase Change Material and Porous Media. *Sustainability* **2023**, *15*, 6439. <https://doi.org/10.3390/su15086439>

Academic Editor: Ramchandra Poda

Received: 12 March 2023

Revised: 2 April 2023

Accepted: 4 April 2023

Published: 10 April 2023



**Copyright:** © 2023 by the authors. Licensee MDPI, Basel, Switzerland. This article is an open access article distributed under the terms and conditions of the Creative Commons Attribution (CC BY) license (<https://creativecommons.org/licenses/by/4.0/>).

## 1. Introduction

The importance and demand for efficient energy storage in all forms of electrical, chemical, and thermal are raising continuously. Several extensive research programs focused on this topic and there are many products available in the market, which mostly belong to the electrical energy storage sector. Thermal energy storage in the form of latent heat storage attracted a lot of attention, mainly due to the following 3 advantages:

- It can reduce peak demand and level demand by storing energy when there is less demand and releasing it when there is high demand.
- It also can minimize heat loss due to the fact that it requires a smaller space, and remove the stratification condition in the storage place.

- It makes the end-user able to control the heat release intensity and rate of heat transfer to the working fluid.

One of the applications for thermal energy storage in the form of latent heat storage is using solar energy sources for hot water production, which could be used for domestic applications and solar heat industrial processes (SHIP). Numerous solar water heating (SWH) systems are currently available in the market. One of the earliest and most well-known forms of SWH systems is the flat plate heat collector. The alternative, more modern, and contemporary method is based on using an evacuated glass tube with a circular aluminum fin in conjunction with either a U-shaped pipe or a heat pipe. The future generation of the SWH systems is designed to be used in conjunction with latent heat thermal energy storage (LHTES) tank that includes PCM [1].

Current SWH systems have several shortcomings and inefficiencies, including the fact that the rate of heat transfer between the heat pipe and the cold water is temperature and flow rate dependent, and the stratification effect in hot water tanks has an effect on the total amount of hot water delivered to the end-user. Intensive study over the last decade has resulted in various potential solutions to these difficulties. One of the options is to employ PCM as a component of a thermal energy storage unit. Kaygusuz [2] described the importance of various aspects related to theory, application, marketing, and research activities to determine the performance of SWH-PCM systems. By examining all of the SWH-PCM systems proposed by researchers, 3 distinct types can be identified: PCM integrated as a back layer into a solar flat plate collector, PCM integrated into an evacuated tube heat pipe solar collector (ETHPSC), and PCM integrated as an intermediate storage layer between the ETHPSC and cold water. Amagour et al. [3] investigated the heat transfer characteristics of a small finned-tube heat exchanger used in the LHTES tank. They performed parametric analyses to determine the influence of the input temperature of the heat transfer fluid (HTF), the flow velocity, and the number and location of fins on charging and discharging performance. It has been shown that increasing the number of fins decreases melting time and increases storage capacity. Alptekin and Ezan [4] investigated the charging performance of the solar-aided packed bed LHTES system. The LHTES tank is integrated with a flat plate solar collector to consider the effect of solar energy. A packed bed PCM is considered in this design. They discovered that reducing the capsule diameter while raising the HTF mass flow rate improves system performance. Pawar and Sobhansarbandi [5] integrated PCM into the heat pipe solar collector (HPSC) cylindrical evacuated tube and simulated the model in 2 phases with and without PCM. The maximum temperature of the heat pipe (HP) without PCM is  $\sim 138$  °C, while for the system with PCM is only  $\sim 90$  °C, which shows that some portion of absorbed solar radiation is stored in the PCM. Therefore, by integrating the tubes with PCM, the issue of overheating the HP can be solved. The PCM-based solar water heater system allows the operation of the system for a longer period when solar radiation is not available.

The advantages of LHTES include high storage density and charging/discharging at a constant temperature. However, the limited thermal conductivity of PCMs used in LHTES is their principal drawback. There are a few solutions to improve this limitation, such as using fins to increase the heat transfer through the PCM [6], encapsulating the PCM to increase the heat transfer surface [7], mixing with high thermal conductivity nanoparticles [8], and using high thermal conductivity porous media as an interface layer to accelerate the heat transfer process [9]. By paying attention to the current technologies of manufacturing porous media products, the cost and quality of manufacturing are reduced significantly. Therefore, using porous products become viable. Porous media in PCMs improves the temperature field's uniformity and reduces the PCM's melting time. Rabbi and Asif [10] studied numerically a configuration of the LHTES module based on the packed bed of encapsulated PCM integrated with copper mesh as porous media. The results indicated that when the water was used as HTF, it took 11 hours to completely charge the system. Whereas, the charging time for R-134 and R-22 was 8.75 and 8.4 h, respectively. The copper mesh increases the heat transfer rate into the PCM. Tiari and

Mahdavi [11] numerically studied the thermal characteristics of an LHTES tank with PCM embedded in highly conductive porous media. A copper foam porous media is utilized to increase heat transfer, impregnated with PCM potassium nitrate ( $\text{KNO}_3$ ). The results were compared with finned heat pipes and it was demonstrated that using porous media is more effective in the charging/discharging modes of PCM. It was shown that the porosity of the metal foam plays a key role in the thermal behavior of the system during the charging and discharging processes. Chen et al. [12] studied a rectangular-shaped container with triangular-shaped twin fins filled with vertically orientated PCM. Nine distinct examples were evaluated for the inquiry, including one pure PCM, 3 nano-PCMs, 2 porous-PCMs, and 3 nano/porous-PCMs. Individual use of porous media was found to increase melting performance significantly. However, adding nanoparticles to enclosures with porous media deteriorates the melting performance of the PCM enclosure. The porosity of the metal foam was found to have an important influence on the PCM's thermal behavior.

In the earlier experimental research works by the same researchers, an LHTES tank was designed to store the absorbed solar heat [6,13,14]. To enhance the heat transfer through PCM, a series of flat fins was fabricated and placed on the heat pipe condenser and another series of spring fins was placed on the cold water pipe inside the tank. The fins successfully increase the heat transfer through PCMs but create a few problems like non-uniform temperature distribution into the PCM and difficulty of fabrication/installation of appropriate fins inside the LHTES tank. According to the findings from the pieces of literature and previous owned research works, using porous media has some preferences in comparison with fins such as the higher rate of heat transfer into the PCM, the more uniform temperature distribution inside the PCM, and easier/cheaper manufacturing of the LHTES tank. This paper experimentally tested a new configuration of the LHTES tank, using ETHPSC with PCM and porous media, to improve the heat transfer in PCM in charging/discharging processes. According to the conducted literature reviews, there is no experimental field test of the LHTES tank incorporating PCM and porous media at the same time.

## 2. System Description

The heat pipe condenser (HPC) is placed into a socket welded to the manifold in a baseline evacuated tube heat pipe solar collector (ETHPSC-B). Solar energy absorbed by the heat pipe evaporator (HPE) of each HP is transferred to the condenser section. The water gets heated as it passes through the HPC. After that, the solar energy is transferred to the water and stored the hot water in an insulated water tank. Then, the end-user picks up the hot water from the water tank.

The proposed evacuated tube heat pipe solar collector with thermal battery (ETHPSC-TM) system reshapes the manifold into a tank and fills it with PCM and porous medium, with the PCM acting as the LHTES material and the porous medium acting as an intermediary heat transfer layer between HPC and PCM. The porous medium is used to increase the heat flux from the HP to the PCM and overcome the low thermal conductivity of the PCM. The porous medium is connected to the HP condenser to collect the heat and distribute it equally throughout the PCM filling the pores. This design of the manifold acts as the LHTES tank, which we call it thermal battery. Another set of pipes is inserted into the LHTES tank to release the stored heat in the PCM to the cold water. The conceptual design of the proposed ETHPSC-TM is shown in Figure 1.

The thermal battery is coupled to an array of ETHPSCs. The HPC is fitted into socket tubes welded to the thermal battery. Sockets are located inside porous media. The PCM is then used to store the heat (charging). The thermal battery heats the incoming cold water through pipes (discharging). A small cavity is designed at the entrance and exit of the cold water and hot water. The cold water cavity is to provide uniform water flow in both pipes. The hot water cavity prevents any vapor from entering the exit pipe. The 3D design of the structure of the thermal battery is shown in Figure 2.

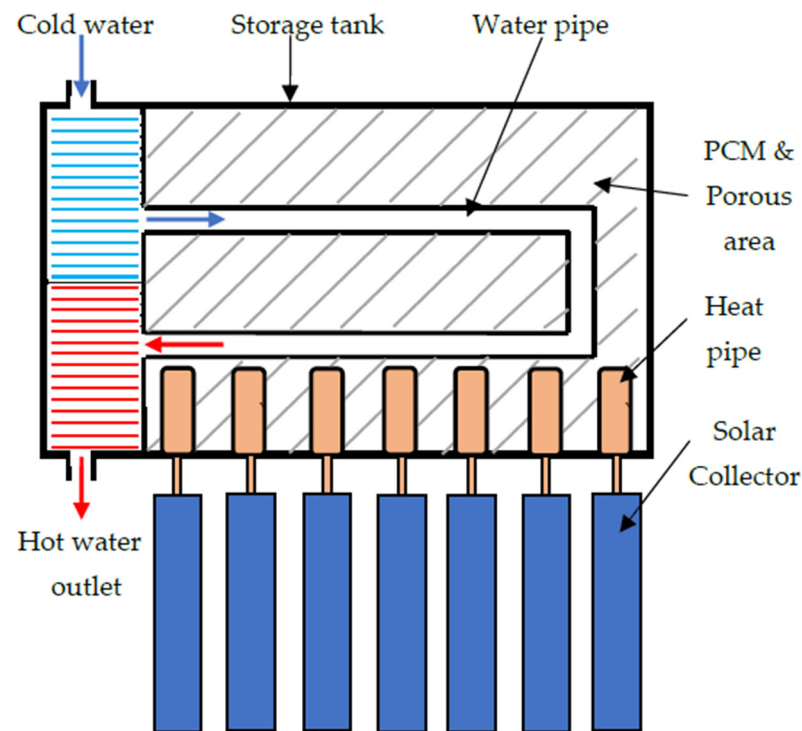


**Figure 1.** Schematic diagram of the ETHPSC with PCM and Porous Medium.

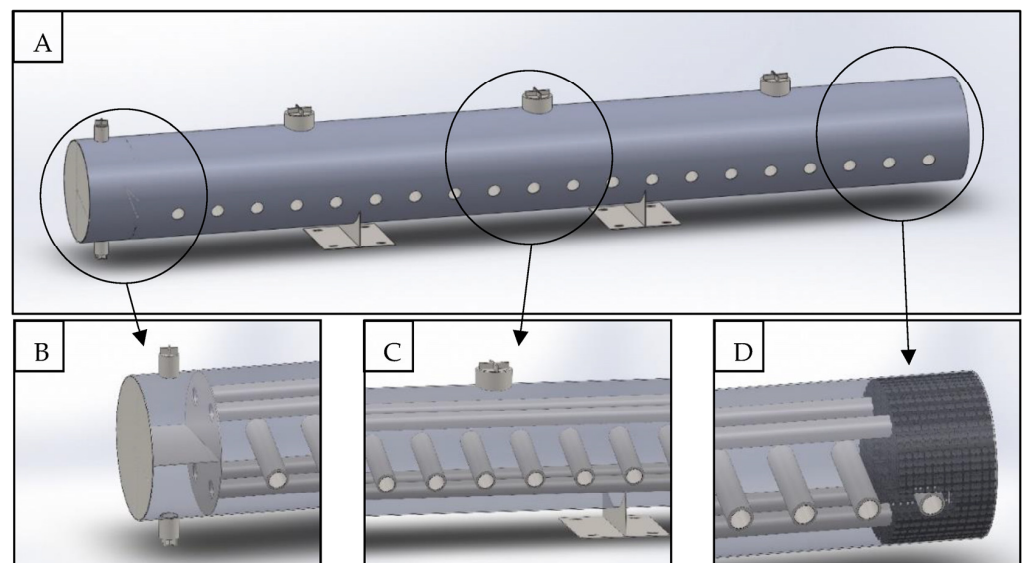


**Figure 2.** (A) 3D view of the Thermal Battery, (B) Inlet and Outlet sections of the water, (C) PCM inlet valve and HP solar tubes inlet socket, (D) Porous Media inside the thermal battery.

The proposed method uses 3 distinct modes of heat transfer: Absorbing solar energy, charging (melting) the PCM via HPC, and discharging (solidification) of the PCM by heat transfer to the water. Solar energy incident on the ETHPSC is first transported to the HPC. Then, the PCM melts, and heat is stored throughout the charging process. The heat is subsequently removed through cold water supply heat exchanger pipes.

The schematic of the experimental setup of the ETHPSC-TM system is shown in Figure 3. Figure 4 depicts the experimental setup and the thermal battery. Table 1 illustrates the experimental setup's dimensions. The site is located on the roof of the Faculty of Engineering, University of Malaya, Kuala Lumpur (latitude  $3.1^{\circ}$  N, longitude  $101.4^{\circ}$  E).

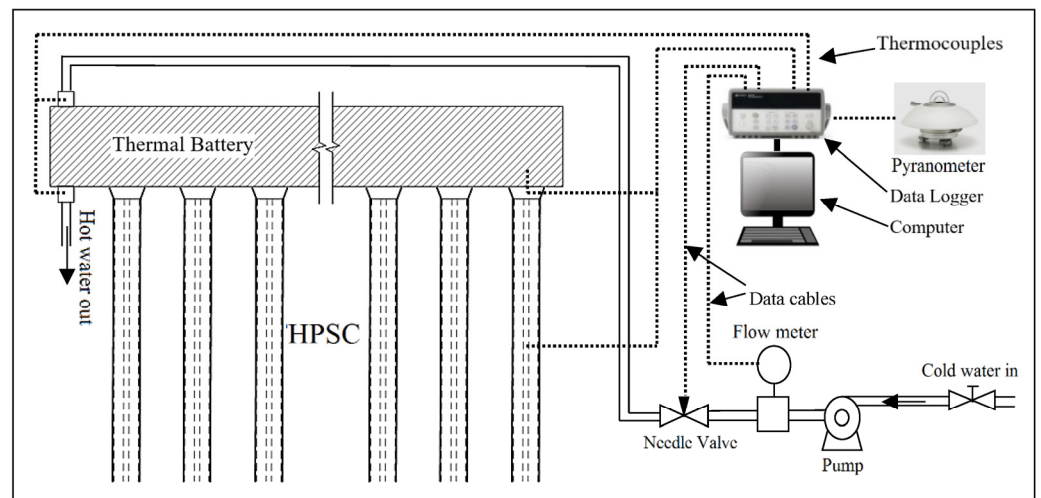


Figure 3. Schematic diagram of the setup.



Figure 4. Photo of the experimental setup.

Table 1. Dimensions of the experimental setup.

Item	Value (mm)
ETHPSC outer tube diameter	58
ETHPSC inner tube diameter	52
Distance between 2 ETHPSCs	142
HPE length	1675
HP adiabatic length	30
HPC length	70
Thermal battery diameter	200
Thermal battery length	1850
Thermal battery wall thickness	2
Water pipe outer diameter	27
Water pipe length (Both U-shape pipes)	~7400

Five important characteristics directly affect the system's performance: the appropriate solar collector, the appropriate solar collector tilt angle, the appropriate PCM selection, the appropriate porous medium selection, and the thermal battery size.

Numerous research investigations have been undertaken in Malaysia to determine the ideal tilt angle for solar systems [15–19]. These study publications advocated for various tilt angles ranging from 10–30 degrees. Ong et al. [20] used 20 degree for the HPSC system. He recommended that, due to the HP's effectiveness being highly dependent on its orientation, The tilt angle of the solar collector should not be too near to the horizontal. In light of this argument and Loh et al. research [21], a tilt angle of 20 degree is recommended.

The desired qualities of an appropriate PCM must be investigated thermodynamically, kinetically, chemically, and economically. The most appealing material for low-temperature heat exchangers and solar applications is Paraffin wax with a melting point of 50–60 °C. [22–27]. Based on an extensive investigation into prior pertinent studies, a Paraffin wax with a melting point of 53–57 °C (ASTM D87) is chosen. A prior study report describes the differential scanning calorimetry of the chosen Paraffin [6]. Table 2 summarizes the thermal characteristics of the Paraffin wax sampled.

**Table 2.** Thermal properties of the Paraffin wax.

Property	Value	Unit
Melting point	53–57 (~55)	°C
Density solid/liquid at 15/70 °C	990/916	kg/m <sup>3</sup>
Thermal conductivity of solid/liquid	0.349/0.167	W/m·K
Specific heat solid/liquid	2.76/2.48	kJ/kg·K
Heat storage capacity	164	kJ/kg

The use of porous media in LHTES systems improves the rate of heat transmission within the PCM, decreasing the PCM's charging/discharging time. Typically, porous media are added into the PCM domain to boost heat conductivity, and the whole phase change process can be hastened due to the PCM domain's higher conduction capabilities. Table 3 summarizes the features of the porous media that were chosen. Figure 5 shows a unit of the chosen porous media.

**Table 3.** Thermal properties of the Silicon Carbide porous media.

Property	Value	Unit
Diameter	200	mm
Thickness	30	mm
PPI	10	-
Porosity	~90	%
Thermal conductivity (100 °C) [28]	~56	W/(m·K)

The tank and pipe materials are mild steel with thermal conductivity of 45 W/(m·K). The size of the LHTES tank may be determined by the average daily solar radiation and the specifications of the solar collector and selected PCM. In Malaysia, the average daily solar radiation on a sunny day is around 4.5 kWh/m<sup>2</sup> per day [20]. Solar radiation that is absorbable by this sort of solar collector is around 65% [14]. A single ETHPSC has a collector area of 0.089 m<sup>2</sup> (a total of 20 ETHPSCs) (1.77 m<sup>2</sup>). As a result, the total solar energy that may be absorbed is approximately 18.6 MJ/day. According to the PCM characteristics in Table 2 and the absorbable solar energy, if the PCM is initially at a temperature of 25 °C, the quantity of PCM that might be melted is approximately 76.6 kg. By considering the porosity of the Silicon Carbide, the volume of the water pipe, the capacity of the HPC sockets, potential energy losses from the tank, solar energy fluctuation, and safety issues,

the PCM should be around 60% of the computed mass above or roughly 46 kg. The size of the LHTES tank must be such that this amount of PCM is filled in liquid form. As a result, the LHTES tank is 0.2 m in diameter and 1.75 m in length. The total number of Silicon Carbide porous media used in the tank is 60 pieces.



**Figure 5.** Photo of the porous media.

The cold water source for the intake is a city water pipe. A low-power sealless centrifugal magnetic water pump provides appropriate pressure for the water supply. A needle valve is installed after the pump to ensure a precise flow rate. Insulation for the thermal battery is by 25 mm thickness Rockwool, while the connection pipe has K-FLEX cool insulation. Copper-constantan thermocouples (TCs) (Type T) are used to monitor temperatures. The TCs' positions are depicted in Figure 3. Temperatures at the water entry and exit were determined using 2 TCs located at the entry and exit of the water pipes in the thermal battery. The Pyranometer is coupled to a TC. A second TC is attached to the flowmeter. One HP is chosen to monitor the condenser and evaporator portions. Tie wires were used to link the TCs to the surfaces of the HPs mechanically.

A Kipp & Zonen Pyranometer (CMP10) measures solar radiation. Burkert inline fitting type S030 is used to determine the water flow rate. The Agilent 34970A data recorder was used to gather all data. For 2006–2009, meteorological data prove that the mean monthly wind speed at the height of 46.2 m above ground level in the Petaling Jaya region of the field test is between 1.5 and 2.0 m/s [29]. As a result, the influence of wind on the system's performance is insignificant.

### 3. Uncertainty Analysis

An uncertainty analysis was conducted by summing the calibration errors of the most influential parameters to set plausible bounds on the accuracy of the reported results. As a result, the following parameters are thought to have a significant impact on the overall thermal efficiency of the systems:

$$\eta = f(\dot{I}, T_{hp,e}, T_{hp,c}, T_m, L_{pcm}, T_{w,h}, T_{w,c}, \dot{m}_w) \quad (1)$$

Each measurement's standard uncertainty may be expressed numerically as [30]:

$$\sigma = \sqrt{\left[ \left( \frac{\delta X_1}{X_1} \right)^2 + \left( \frac{\delta X_2}{X_2} \right)^2 + \dots + \left( \frac{\delta X_n}{X_n} \right)^2 \right]} \quad (2)$$

where  $n$  is the number of parameters that affect the accuracy of the results,  $\frac{\delta X_i}{X_i}$  corresponds to the parameters' relative uncertainty.

All TCs were calibrated, and temperatures were assessed to be within a range of 30–150 °C. The measured temperature errors of the TCs for HPE, HPC, and inlet/outlet supply water pipes are  $\pm 4.7\%$ ,  $\pm 3.9\%$ ,  $\pm 4.3\%$ , and  $\pm 4.4\%$ , respectively. The same data for the flowmeter and Pyranometer is  $\pm 0.2\%$  and  $\pm 1.4\%$  of reading of ampere in the range of 4–20 mA, respectively. The PCM's melting point and latent heat capacity are off by  $\pm 4.7\%$  and  $\pm 1.4\%$ , respectively. Using these data and the aforementioned calculation, the uncertainty in the system's overall thermal efficiency may be estimated to be around 9.3%.

#### 4. Results and Discussions

The proposed system is intended to be used for a domestic hot water production application. There are 20 HPSCs in the setup. All HPSCs together have a total aperture area of 0.089 m<sup>2</sup> (1.77 m<sup>2</sup>). The tap water is heated in the thermal battery before being sent to the end-user. Two sets of experiments were conducted to understand the system's performance better. The field tests are taken during August and September.

**Mode 1:** Charging/discharging mode. This test aims to find out the total absorbable solar radiation and total energy transfers to cold water. By this test, the efficiency of the system could be estimated. The experiment was conducted during the daytime and evening time. The charging period begins in the morning and ends at about 5 p.m. Then, the discharge (water draw-off) starts after 5 p.m., until midnight. The flow rate is 60 L/h (lph).

**Mode 2:** Periodic draw-off. The purpose of this test is to determine the highest and average hot water temperatures throughout the morning and evening draw-offs. The experimental test was carried out in the morning and evening, according to the plan shown in Figure 6. The draw-off was performed 4 times in the morning and 4 times in the evening. The draw-off duration is for 5 min with 10 min intervals and a 2 L/min (lpm) flow rate.

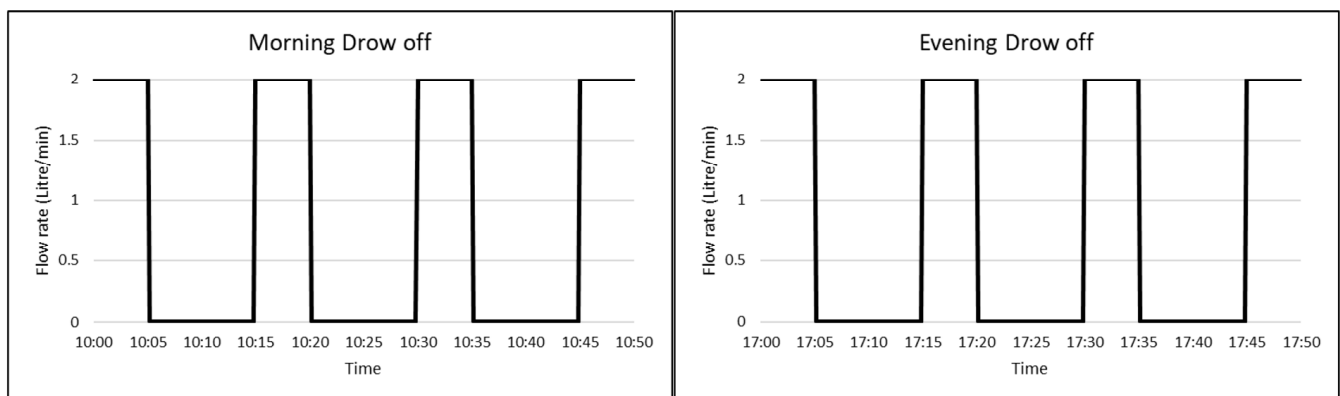


**Figure 6.** Water draw-off pattern and flow rate.

##### 4.1. Mode 1 (Charging-Discharging Mode)

Solar radiation impacts the ETHPSC while it is in charging mode only, and the heat is absorbed and delivered to the thermal battery via the HPs, melting the PCM. The PCM retains heat in the form of latent and sensible heat. The supply water does not pass through the thermal battery in charging mode. During the discharge mode, tap water flows through the pipes and is heated by the melted PCM. When solar radiation is inadequate, this mode is enabled, and heat transfer between the ETHPSC and the thermal battery is minimal or non-existent. Heat transfer happens in just one direction in the HP adiabatic section (HPA) to the HPC [31] Table 4 present the summary of the solar intensity level and weather condition of the day for 4 runs of the mode 1.

**Table 4.** Summary of the runs for mode 1.

Run No.	Solar Intensity Category	Weather Conditions in Morning, Noon, Afternoon
#1	Low	cloudy, cloudy, cloudy
#2	Low	sunny, rainy, rainy
#3	High	sunny, sunny, sunny
#4	High	sunny, sunny, sunny

Figure 7 presents the solar radiation graph for 2 low intensity days (runs #1 and #2). The hot and cold water graphs are presented on the right side. It shows that when hot water discharge starts at 17:00, the highest temperature is close to 50 °C, but after about 30 min, it drops dramatically to about 36–38 °C. Then, it takes about 1–2 h for that hot water temperature to drop to below 35 °C. It should be highlighted that the cold water temperature also reduces during the discharge time. Initially, the cold water temperature is over 30 °C, but it reduces slowly to 27–28 °C after a while. The graphs on the right side show that the thermal battery can provide at least a 10 °C temperature difference in the first 2 h (17:00–19:00) and at least 5 °C for 2 h after that (19:00–21:00). The rate of hot water temperature reduction is a matter that causes by long continuous water draw-off.

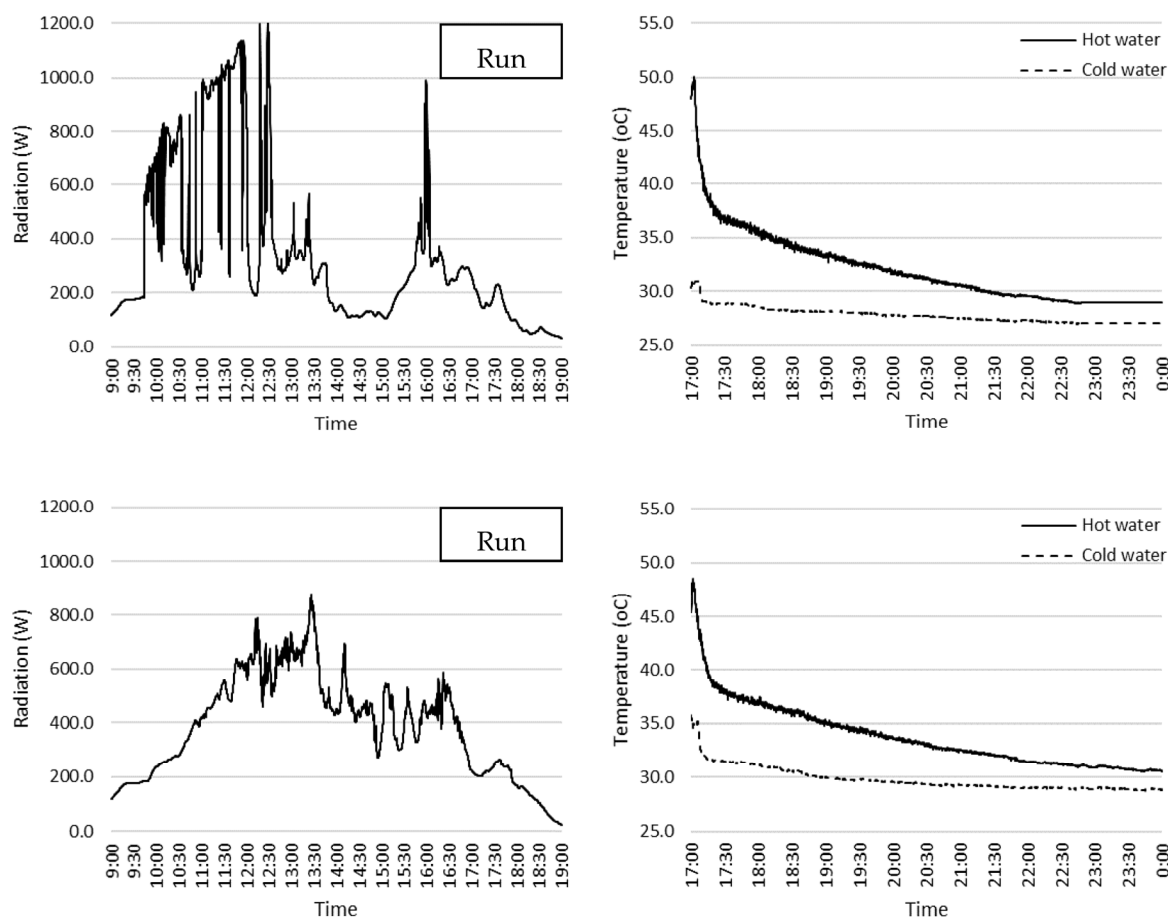


**Figure 7.** Runs #1 and #2 with low intensity solar radiations. (Left) Solar radiation, (Right) inlet/outlet hot water temperatures.

Figure 8 demonstrates the solar radiation for 2 sunny days, although there are many fluctuations in the radiation due to the partial cloudiness (Runs #3 and #4). The hot water and cold water graphs are presented on the right side. When the discharge of hot water starts, the highest recorded temperature is about 55 °C. In run #3, it takes about half an

hour for the temperature of hot water to drop to about 40 °C. It takes about 2 and a half hours to drop to 35 °C. In run #4, it takes about one hour for the temperature of hot water drops to 40 °C, and it takes about 3 h to drop 35 °C. In run #3, the temperature difference is over 10 °C in the first half an hour, and it takes about 2 and half hours to reduce to 5 °C. In run #4, the temperature difference is more than 10 °C in the first hour and is more than 5 °C for the next 3 h. This temperature profile shows that the thermal battery is able to provide enough hot water with continuous draw-off for about 3–4 h, which is long enough for normal use.

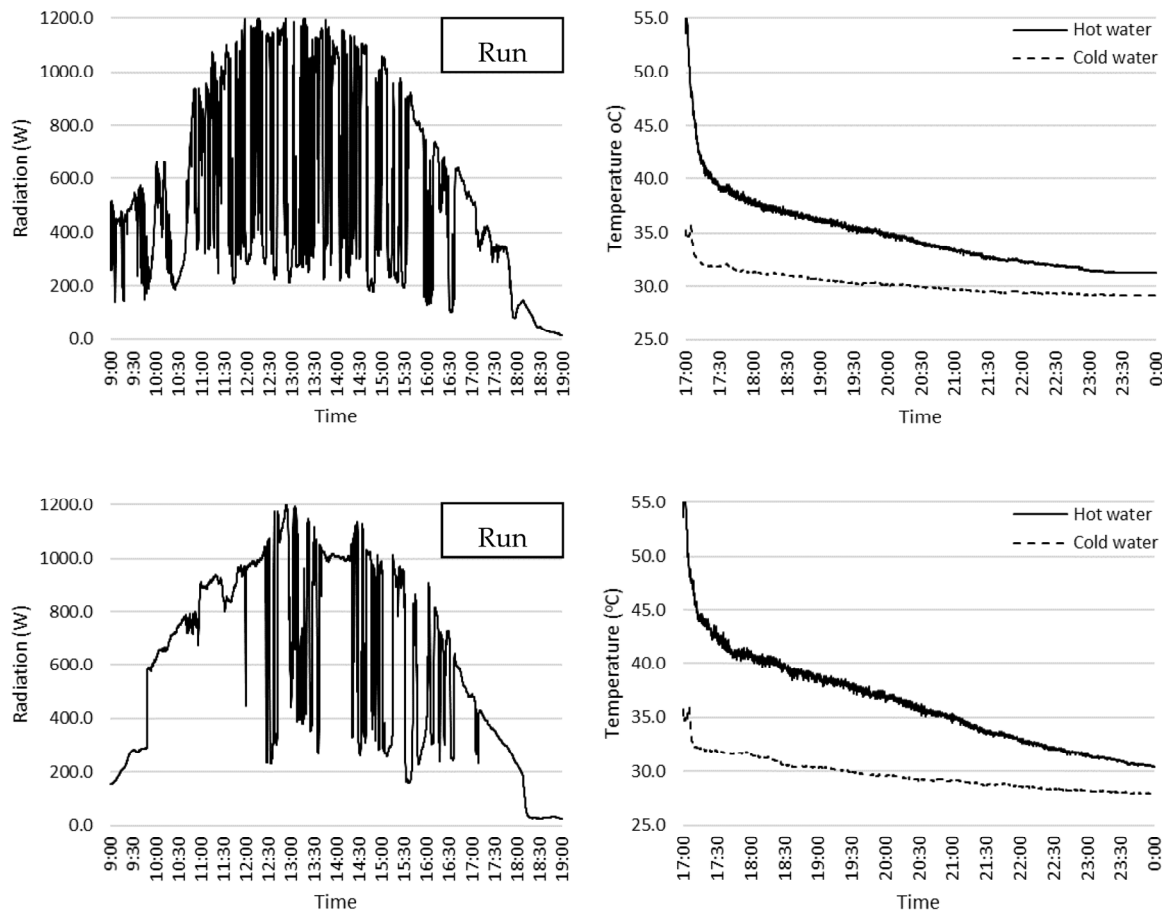


**Figure 8.** Runs #3 and #4 with high intensity solar radiations. (Left) Solar radiation, (Right) inlet/outlet hot water temperatures.

#### Efficiency of the Thermal Battery

The important aspect of comprehending the thermal battery's performance is determining the thermal efficiency. Regarding the design of the thermal battery, it is impossible to accurately observe the melt fraction and energy storage in the PCM. As a result, measurement of the system's thermal efficiency is restricted to determining the amount of solar radiation that can be absorbed and the total amount of heat transferred to the cold water. According to the mathematical model introduced by Naghavi et al. [6], the absorbable solar energy in Malaysian weather conditions and solar collector inclination is about 60%. It is also reported that the average heat loss by the HP is 5% ( $\eta_{HP} = 95\%$ ) and the approximate heat loss from the thermal battery is less than 5% ( $q_{loss} = 95\%$ ). Therefore, the storable heat ( $Q_{st}$ ) in the thermal battery can be calculated by the following equation:

$$Q_{st} = \left( \sum \dot{I} \times A_{sc} \right) \times \eta_{HP} \times q_{loss} \quad (3)$$

which,  $\dot{I}$  is recorded solar radiation data,  $A_{sc}$  is the total solar collector area,  $\eta_{HP}$  is the thermal efficiency percentage of the HP, and  $q_{loss}$  is the percentage of the storable heat of the thermal battery.

Heat convection to the stream of supply water ( $Q_w$ ) can also be computed from [32]:

$$Q_w = \sum \dot{m}_w \cdot c_{p,w} \cdot (\dot{T}_{w,h} - \dot{T}_{w,c}) \quad (4)$$

which,  $\dot{m}_w$  is the water flowrate,  $c_{p,w}$  is the specific heat of water,  $\dot{T}_{w,h}$  is the hot water temperature, and  $\dot{T}_{w,c}$  is the cold water temperature.

The proportion of the energy transferred to the supply water and the storable thermal energy express the thermal efficiency of the thermal battery ( $\eta_{TB}$ ):

$$\eta_{TB} = \left( \frac{Q_w}{Q_{st}} \right) \times 100\% \quad (5)$$

The proportion of the energy transferred to the supply water and the recorded total solar radiation express the total thermal efficiency of the system:

$$\eta_s = \left( \frac{Q_w}{\sum \dot{I} \times A_{sc}} \right) \times 100\% \quad (6)$$

The summary of the 4 runs is shown in Table 5.

**Table 5.** Cumulative energy and efficiencies from Runs 1–4.

Runs No.	Daily Radiation (MJ/m <sup>2</sup> )	Daily Total Solar Radiation (MJ)	Storable Daily Solar Radiation (MJ)	Total Heat Transfer to Water (MJ)	Efficiency of Thermal Battery (%)	Efficiency of System (%)
#1	13.9	24.6	13.3	5.8	44%	24%
#2	12.3	21.8	11.8	5.5	47%	25%
#3	18.6	33.0	17.9	7.6	42%	23%
#4	21.4	37.9	20.5	11.4	56%	30%

As indicated in Table 5 and Figure 9, the thermal efficiency of the thermal battery is in the range of 44% on low solar intensity days and 56% on high solar intensity days (average 50%). By considering the uncertainty of the results and plotting a linear trendline, it could be understood that the fluctuation of the efficiency of the thermal battery is not more than  $50\% \pm 9.3\%$  in different weather conditions.

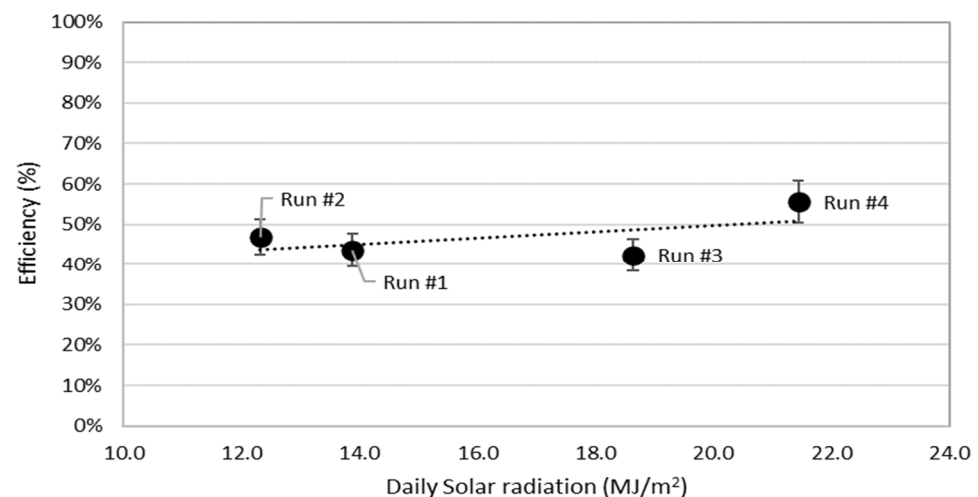


**Figure 9.** Overall thermal efficiency variations of the thermal battery with uncertainty range.

One phenomenon that is derived from the results is that during heat transfer to the cold water, the adjacent layer of the PCM solidifies sooner, and due to the lower thermal conductivity of the solid PCM, the direct heat transfer rate from PCM to the cold water pipe is reduced. This situation is controlled by the porous media, which boosts heat transfer from remained melted PCM to the cold water pipe.

#### 4.2. Mode 2 (Periodic Draw-Off Mode)

This mode depicts a batch-wise concurrent charging-discharging procedure to determine the system's compliance with user demand. The significance of this mode becomes clear when one considers how many research studies investigated their system over a single day or in a continuous discharge pattern. Therefore, besides mode 1, mode 2 of runs #5–#8 was executed to observe the performance of the thermal battery in different climatic conditions and different times of hot water draw-off.

Numerous pieces of research concentrated on the volume of hot water withdrawn from the SWH system. In Malaysia's metropolitan regions, the typical household size is 3–5 people, and each person requires 25–30 L of hot water at operating temperature [33]. Operating temperature is the minimum useable temperature of hot water for domestic applications such as showering. The recommended operating temperature for domestic use is at least 38 °C [34]. The optimal daily hot water capacity at operational temperature for a family in Malaysia is between 100–120 L per day (lpd). The hot water flow rate from the thermal battery is fixed to be 2 L per minute, which in case of being over 38 °C will be mixed with cold water to determine the total producible hot water magnitude.

The graphs of solar intensity are shown in Figure 10. Runs were carried out in 4 days, of which 2 days are in low solar intensity and the other 2 days are in high solar intensity conditions. Figure 11 presents runs #5 and #6. The draw-off was performed 4 times in the morning and 4 times in the evening, the morning draw-off is depicted in the left side graph, and the evening draw-off is depicted in the right side graphs. In run #5, morning draw-off, the hot water temperature is mostly less than 35 °C. In the evening draw-off, the hot water temperature is also in the range of 35 °C. The results indicate that on days with low solar intensity, the thermal battery can warm the water at least 3–5 °C in the morning and 5–10 °C in the evening. This size of the thermal battery or type of PCM cannot independently provide hot water at the operating temperature on cloudy or rainy days. It needs to be more prominent in size, optimize the PCM, or coupled with an auxiliary electrical heater to level up the output hot water temperature.

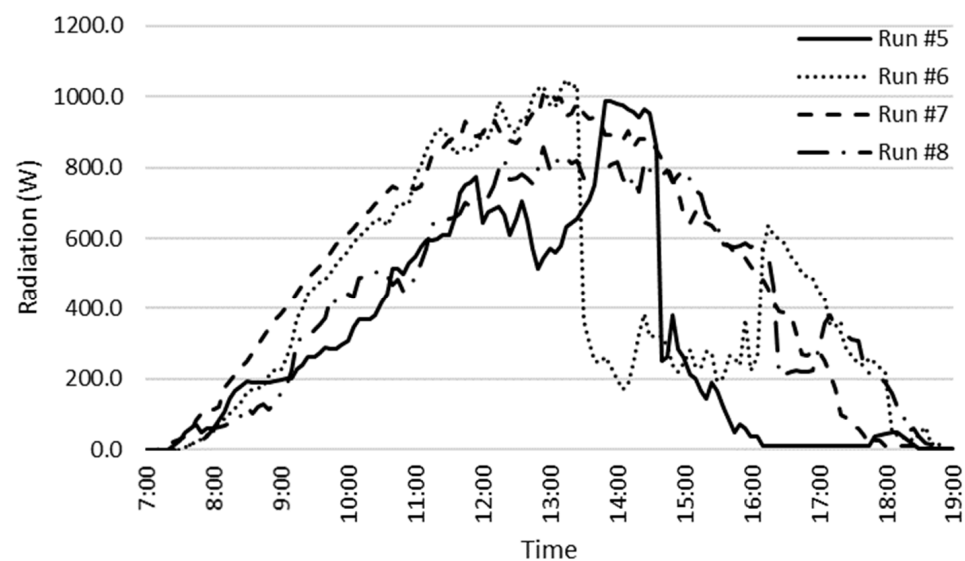
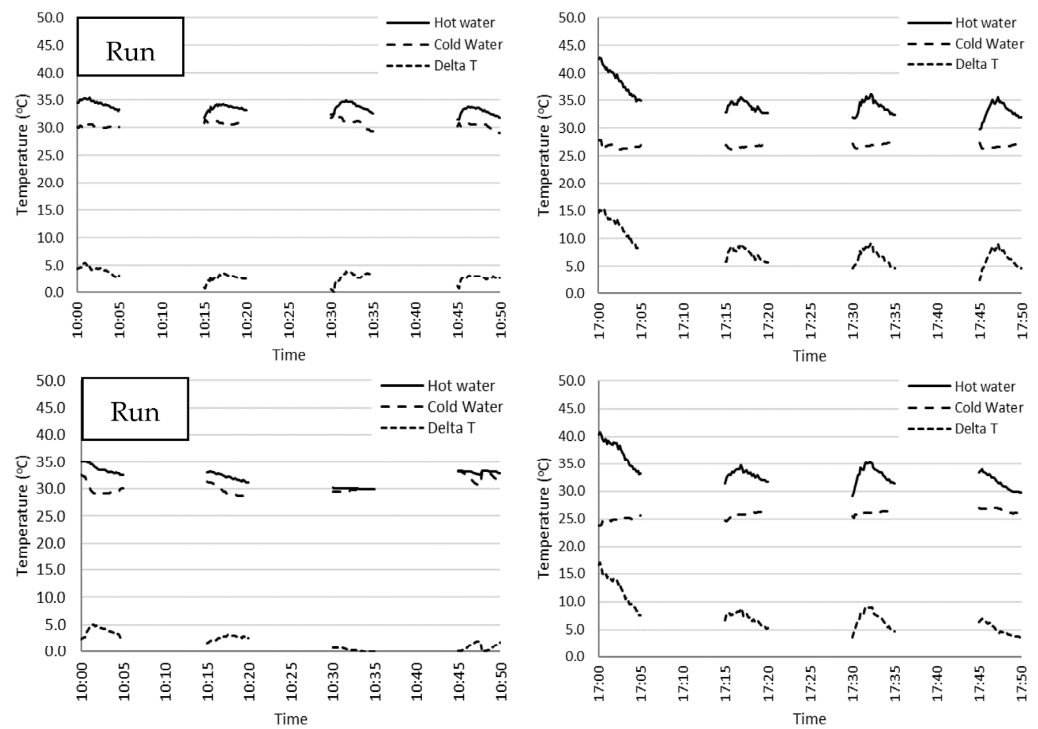
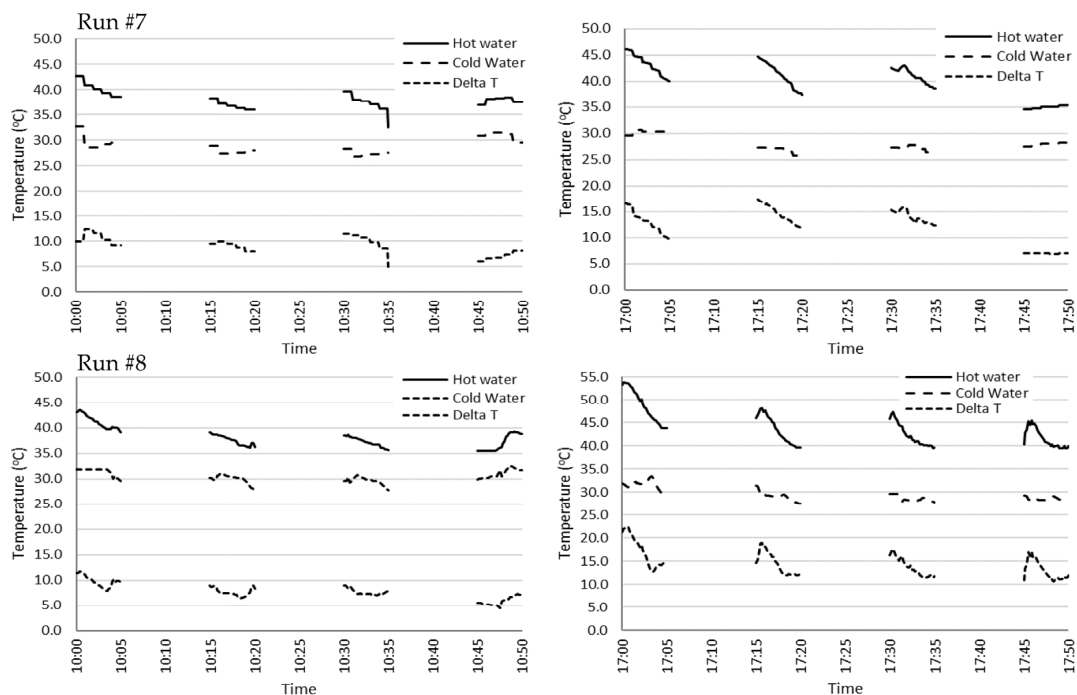


Figure 10. Solar radiation for 4 Runs in Mode 2.



**Figure 11.** Runs #5 and #6 for low solar radiation intensity days. Water draw-off in the morning (Left). Water draw-off in the evening (Right).

The results of runs #7 and #8 are depicted in Figure 12. These 2 runs are for high solar intensity days. In the morning, the hot water draw-off temperature is often greater than 38–40 °C, and in the evening, the hot water temperature is typically between 40–45 °C. On days with high solar intensity, the thermal battery may heat the cold water to a minimum of 10 °C in the morning and 15 °C in the evening. On sunny days, the thermal battery can provide hot water at an operational temperature.



**Figure 12.** Runs #7 and #8 for high solar radiation intensity days. Water draw-off in the morning (Left). Water draw-off in the evening (Right).

### Hot Water Volume

Armstrong [35] defined hot water volume in operating temperature ( $V_u$ ) as equal to the volume of hot water output ( $T_{w,o}$ ) in recorded temperature that can be mixed with cold water ( $T_{w,i}$ ) to determine a useful final operating temperature ( $T_u$ ), which is 38 °C. The hot water volume in operating temperature is determined by:

$$V_u = m_w \times \sum \frac{T_{w,o}(t) - T_u}{T_u - T_{w,i}(t)} \quad (7)$$

Table 6 expresses the daily solar radiation (as explained in mode 1) and hot water volume in the operating temperature for runs #5–#8. The data also explains the results of the graphs. On days with low solar intensity, the thermal battery cannot maintain the hot water's operational temperature. However, on days with high solar intensity, the thermal battery can provide enough hot water for routine home usage at an operating temperature suitable for a family of 3–5 persons in Malaysia.

**Table 6.** Runs #5–#8, daily solar radiation and producible hot water at operating temperature.

Run No.	Recorded Daily Solar Radiation ( $I_r/m^2$ )	Total Daily Solar Radiation ( $I_t/Day$ )	Absorbable Daily Solar Radiation ( $I_a/Day$ )	Hot Water Volume in 38 °C (L/Day)
#5	13.6	24.1	13.1	0.0
#6	15.9	28.2	15.3	0.0
#7	22.1	39.2	21.2	197.1
#8	20.1	35.5	19.2	130.8

If the thermal battery is not fully discharged in the evening, the battery would be able to provide hot water in the morning with the leftover heat from the previous day. This system can keep the stored heat from the previous day to produce hot water in the early morning for domestic usage.

### 5. Conclusions

The performance of the ETHPSC-TM system in 2 distinct modes was investigated experimentally under real field circumstances. The thermal battery consists of a PCM for thermal energy storage and a series of porous media plates to enhance heat transfer from the solar collector and overcome the low thermal conductivity of the PCM. The porous media is connected to the HPC to collect the heat and distribute it uniformly throughout the PCM filling the pores. To assess the thermal performance of this system, experimental data were collected from morning to evening in various weather conditions days.

The result indicated that:

1. The efficiency of the thermal battery is in the range of 44% on low solar intensity days and 56% on high solar intensity days.
2. Considering the solar radiation fluctuation and uncertainty of the results, the overall efficiency of the thermal battery is 50% ± 9.3%.
3. The thermal battery can warm up the cold water higher than the operating temperature on a sunny day (more than 120 L per day at 38 °C).
4. The thermal battery required an auxiliary heater to warm up the outlet water to the operating temperature on cloudy or rainy days.

The main advantages of this system design over current products are as below:

- a. This configuration does not need any separate hot water storage tank.
- b. There is no need for a water pump to increase the hot water pressure.
- c. The effect of layering of hot water (stratification effect) in the hot water tank is removed.
- d. Hot water can be produced immediately according to the demand of the end-user.

- e. The thermal battery is connected to the solar collector. Removing the hot water tank, extra pipe, and water pump makes the system compact, cheaper, and easy to install.
- f. Using porous media provides better heat distribution in the PCM.

**Author Contributions:** Conceptualization, M.S.N.S. and S.M.M.G.; Validation, M.S.N.S. and S.M.M.G.; Writing—original draft, M.S.N.S.; Writing—review & editing, M.S.N.S., M.S., B.C.A., H.S.C.M., S.M.M.G. and Y.N.; Supervision, H.S.C.M. and Y.N. All authors have read and agreed to the published version of the manuscript.

**Funding:** This research was funded by Universiti Malaya under the Postdoctoral Grant and the Fundamental Research Grant Scheme (FP048-2019A).

**Institutional Review Board Statement:** Not applicable.

**Informed Consent Statement:** Not applicable.

**Data Availability Statement:** Data is contained within the article.

**Acknowledgments:** The authors would like to acknowledge the University of Malaya for financial support and Energy Modelling and Sustainable Energy System (METSAP) research laboratory at the faculty of New Sciences and Technologies, the University of Tehran to support completion of this research.

**Conflicts of Interest:** The authors declare no conflict of interest.

## Nomenclature

### Symbols

$A_{tank}$	LHS tank Surface area
$A_{sc}$	Solar collector apparatus area
$c_{p,w}$	Heat capacity of water
$f$	Function
$F_{melt}$	Molten PCM fraction
$\dot{I}$	incident radiation
$L$	Latent heat energy
$\dot{m}_w$	Water mass flowrate
$m_w$	Total mass of hot water
$N_f$	Number of the fins
$N_t$	Number of HPSCs
$q_{loss}$	Heat loss from the tank
$Q_{st}$	Heat storage
$Q_w$	Heat transfer to the cold water
$V_u$	hot water volume in operating temperature
$S$	Absorbed solar energy
$T$	Temperature

### Greek

$\sigma$	Uncertainty measurement
$\eta$	Efficiency

### Abbreviations

ETHPSC	Evacuated tube HP solar collector
HP	Heat pipe
HPA	Heat pipe adiabatic
HPC	Heat pipe condenser
HPE	Heat pipe evaporator
HPSC	Heat pipe solar collector
HTF	Heat transfer fluid
LHTES	Latent heat thermal energy storage
PCM	Phase change materials
PV	Photovoltaic
SHIP	Solar heat industrial processes
SWH	Solar water heating
TC	Thermocouple

## References

1. Naghavi, M.; Metselaar, H.; Ang, B.; Zamiri, G.; Esmailzadeh, A.; Nasiri-Tabrizi, B. A critical assessment on synergistic improvement in PCM based thermal batteries. *Renew. Sustain. Energy Rev.* **2021**, *135*, 110259. [[CrossRef](#)]
2. Kaygusuz, K. Experimental and theoretical investigation of latent heat storage for water based solar heating systems. *Energy Convers. Manag.* **1995**, *36*, 315–323. [[CrossRef](#)]
3. Amagour, M.E.H.; Bennajah, M.; Rachek, A. Numerical investigation and experimental validation of the thermal performance enhancement of a compact finned-tube heat exchanger for efficient latent heat thermal energy storage. *J. Clean. Prod.* **2021**, *280*, 124238. [[CrossRef](#)]
4. Alptekin, E.; Ezan, M.A. A systematic assessment on a solar collector integrated packed-bed single/multi-layered latent heat thermal energy storage system. *J. Energy Storage* **2021**, *37*, 102410. [[CrossRef](#)]
5. Pawar, V.R.; Sobhansarbandi, S. CFD modeling of a thermal energy storage based heat pipe evacuated tube solar collector. *J. Energy Storage* **2020**, *30*, 101528. [[CrossRef](#)]
6. Naghavi, M.; Ong, K.; Badruddin, I.; Mehrali, M.; Metselaar, H. Thermal performance of a compact design heat pipe solar collector with latent heat storage in charging/discharging modes. *Energy* **2017**, *127*, 101–115. [[CrossRef](#)]
7. Silakhori, M.; Naghavi, M.S.; Metselaar, H.S.C.; Mahlia, T.M.I.; Fauzi, H.; Mehrali, M. Accelerated Thermal Cycling Test of Microencapsulated Paraffin Wax/Polyaniline Made by Simple Preparation Method for Solar Thermal Energy Storage. *Materials* **2013**, *6*, 1608–1620. [[CrossRef](#)]
8. Mehrali, M.; Latibari, S.T.; Mehrali, M.; Mahlia, T.M.I.; Metselaar, H.S.C.; Naghavi, M.S.; Sadeghinezhad, E.; Akhiani, A.R. Preparation and characterization of palmitic acid/graphene nanoplatelets composite with remarkable thermal conductivity as a novel shape-stabilized phase change material. *Appl. Therm. Eng.* **2013**, *61*, 633–640. [[CrossRef](#)]
9. Yang, X.; Yu, J.; Guo, Z.; Jin, L.; He, Y.-L. Role of porous metal foam on the heat transfer enhancement for a thermal energy storage tube. *Appl. Energy* **2019**, *239*, 142–156. [[CrossRef](#)]
10. Rabbi, J.; Asif, M. A numerical study on effects of heat transfer fluids, copper mesh in packed bed and porosity, on charging time of paraffin based packed bed thermal energy storage. *Energy Storage* **2021**, *3*, e254. [[CrossRef](#)]
11. Tiari, S.; Mahdavi, M. Computational study of a latent heat thermal energy storage system enhanced by highly conductive metal foams and heat pipes. *J. Therm. Anal. Calorim.* **2020**, *141*, 1741–1751. [[CrossRef](#)]
12. Chen, S.-B.; Saleem, S.; Alghamdi, M.N.; Nisar, K.S.; Arsalanloo, A.; Issakhov, A.; Xia, W.-F. Combined effect of using porous media and nano-particle on melting performance of PCM filled enclosure with triangular double fins. *Case Stud. Therm. Eng.* **2021**, *25*, 100939. [[CrossRef](#)]
13. Naghavi, M.; Ang, B.; Rahmanian, B.; Bazri, S.; Mahmoodian, R.; Metselaar, H. On-demand dynamic performance of a thermal battery in tankless domestic solar water heating in the tropical region. *Appl. Therm. Eng.* **2020**, *167*, 114790. [[CrossRef](#)]
14. Naghavi, M.; Ong, K.; Badruddin, I.; Mehrali, M.; Silakhori, M.; Metselaar, H. Theoretical model of an evacuated tube heat pipe solar collector integrated with phase change material. *Energy* **2015**, *91*, 911–924. [[CrossRef](#)]
15. Fadaeenejad, M.; Mohd Radzi, M.A.; Fadaeenejad, M.; Zarif, M.; Gandomi, Z. Optimization and comparison analysis for application of PV panels in three villages. *Energy Sci. Eng.* **2015**, *3*, 145–152. [[CrossRef](#)]
16. Saadatian, O.; Sopian, K.; Elhab, B.; Ruslan, M.H.; Asim, N. Optimal solar panels' tilt angles and orientations in Kuala Lumpur, Malaysia. In Proceedings of the 1st WSEAS International Conference on Energy and Environment Technologies and Equipment (EEETE'12), London, UK, 27–29 October 2017; pp. 100–107.
17. Khatib, T.; Mohamed, A.; Sopian, K. Optimization of a PV/wind micro-grid for rural housing electrification using a hybrid iterative/genetic algorithm: Case study of Kuala Terengganu, Malaysia. *Energy Build.* **2012**, *47*, 321–331. [[CrossRef](#)]
18. Daut, I.; Irwanto, M.; Irwan, Y.M.; Gomesh, N.; Ahmad, N.S. Clear sky global solar irradiance on tilt angles of photovoltaic module in Perlis, Northern Malaysia. In Proceedings of the International Conference on Electrical, Control and Computer Engineering (INECCE), Kuantan, Malaysia, 21–22 June 2011; IEEE: Piscataway, NJ, USA, 2011.
19. Elhassan, Z.A.M.; Zain, M.F.M.; Sopian, K.; Awadalla, A. Output Energy of Photovoltaic Module Directed at Optimum Slope Angle in Kuala Lumpur, Malaysia. *Res. J. Appl. Sci.* **2011**, *6*, 104–109. [[CrossRef](#)]
20. Ong, K.S.; Tong, W.L.; Sheriwati, S.; Low, T.H. System performance of heat pipe solar water heaters. In Proceedings of the 10th International Heat Pipe Symposium, New Taipei City, Taiwan, 6–9 November 2011; Tamkang University Press: New Taipei City, Taiwan, 2011.
21. Loh, C.; Harris, E.; Chou, D. Comparative study of heat pipes performances in different orientations. In Proceedings of the Semiconductor Thermal Measurement and Management IEEE Twenty First Annual IEEE Symposium, San Jose, CA, USA, 15–17 March 2005; IEEE: Piscataway, NJ, USA, 2005.
22. Horbaniuc, B.; Dumitrascu, G.; Popescu, A. Mathematical models for the study of solidification within a longitudinally finned heat pipe latent heat thermal storage system. *Energy Convers. Manag.* **1999**, *40*, 1765–1774. [[CrossRef](#)]
23. Liu, Z.; Wang, Z.; Ma, C. An experimental study on the heat transfer characteristics of a heat pipe heat exchanger with latent heat storage. Part II: Simultaneous charging/discharging modes. *Energy Convers. Manag.* **2006**, *47*, 967–991. [[CrossRef](#)]
24. Liu, X.; Fang, G.; Chen, Z. Dynamic charging characteristics modeling of heat storage device with heat pipe. *Appl. Therm. Eng.* **2011**, *31*, 2902–2908. [[CrossRef](#)]
25. Hussein, H.; El-Ghetany, H.; Nada, S. Experimental investigation of novel indirect solar cooker with indoor PCM thermal storage and cooking unit. *Energy Convers. Manag.* **2008**, *49*, 2237–2246. [[CrossRef](#)]

26. Karthick, R.; Manivannan, A. Thermal energy storage in solar water heater using phase change material. *Int. Dly. J. Discov.* **2015**, *37*, 28–36.
27. Wang, Z.; Qiu, F.; Yang, W.; Zhao, X. Applications of solar water heating system with phase change material. *Renew. Sustain. Energy Rev.* **2015**, *52*, 645–652. [[CrossRef](#)]
28. Technical Data Silicon Carbide. 2021. Available online: [https://global.kyocera.com/prdct/fc/list/material/silicon\\_carbide/silicon\\_carbide.html](https://global.kyocera.com/prdct/fc/list/material/silicon_carbide/silicon_carbide.html) (accessed on 15 October 2021).
29. Chong, W.; Naghavi, M.; Poh, S.; Mahlia, T.M.I.; Pan, K. Techno-economic analysis of a wind–solar hybrid renewable energy system with rainwater collection feature for urban high-rise application. *Appl. Energy* **2011**, *88*, 4067–4077. [[CrossRef](#)]
30. Li, F.-F.; Diao, Y.-H.; Zhao, Y.-H.; Zhu, T.-T.; Liu, J. Experimental study on the thermal performance of a new type of thermal energy storage based on flat micro-heat pipe array. *Energy Convers. Manag.* **2016**, *112*, 395–403. [[CrossRef](#)]
31. Faghri, A. Heat Pipes: Review, Opportunities and Challenges. *Front. Heat Pipes (FHP)* **2014**, *5*. [[CrossRef](#)]
32. Bergman, T.L.; Incropera, F.P. *Introduction to Heat Transfer*; Wiley: New York, NY, USA, 2011.
33. JKR. Standard Specification for Building Works. In *Water Meter*; Jabatan Kerja Jaya: Kuala Lumpur, Malaysia, 2004.
34. Thermostatic Mixing Valve Manufacturers Association. *Recommended Code of Practice for Safe Water Temperatures*; BEAMA: London, UK, 2013.
35. Armstrong, P.; Ager, D.; Thompson, I.; McCulloch, M. Domestic hot water storage: Balancing thermal and sanitary performance. *Energy Policy* **2014**, *68*, 334–339. [[CrossRef](#)]

**Disclaimer/Publisher’s Note:** The statements, opinions and data contained in all publications are solely those of the individual author(s) and contributor(s) and not of MDPI and/or the editor(s). MDPI and/or the editor(s) disclaim responsibility for any injury to people or property resulting from any ideas, methods, instructions or products referred to in the content.